The SDUST2022GRA global marine gravity anomalies recovered from radar and laser altimeter data: Contribution of ICESat-2 laser altimetry

Zhen Li[1], Jinyun Guo[1*], Chengcheng Zhu[2], Xin Liu[1], Cheinway Hwang[3], Sergey Lebedev[4], Xiaotao Chang[5], Anatoly Soloviev[4], Heping Sun[6]

[1] College of Geodesy and Geomatics, Shandong University of Science and Technology, Qingdao 266590, China
[2] School of Surveying and Geo-informatics, Shandong Jianzhu University, Jinan 250101, China
[3] Department of Civil Engineering, National Yang Ming Chiao Tung University, Hsinchu 300, Taiwan
[4] Geophysical Center, Schmidt Institute of Physics of the Earth, Russian Academy of Sciences, Moscow, Russia
[5] Land Satellite Remote Sensing Application Center, Ministry of Natural Resources, Beijing 100048, China
[6] State Key Laboratory of Geodesy and Earth's Dynamics, Innovation Academy of Precision Measurement Science and Technology, Chinese Academy of Sciences, Wuhan 430077, China

Correspondence to: Jinyun Guo (jinyunguo1@126.com)

Abstract. The global marine gravity anomaly model is predominantly recovered from along-track radar altimeter data. Despite significant advancements in gravity anomalies recovery, the improvement of the gravity anomaly model remains constrained by the absence of cross-track geoid gradients and the reduction of radar altimeter data, especially in coastal and high-latitude regions. ICESat-2 laser altimetry, with three-pair laser beams configuration, small footprint, and near-polar orbit, facilitates the determination of cross-track geoid gradients and provides valid observations in certain regions. We presents an ICESat-2 altimeter data processing strategy, including the determination of cross-track geoid gradients and the combination of along-track and cross-track geoid gradients. Utilizing these methods, we developed a new global marine gravity model, SDUST2022GRA, from radar and laser altimeter data. Different weight determination method were applied to each type of altimeter data.The precision and spatial resolution of SDUST2022GRA were assessed against published altimeter-derived global gravity anomaly models (DTU17, V32.1, NSOAS22) and shipborne gravity measurements. SDUST2022GRA achieved a global precision of 4.43 mGal, representing an improvement of approximately 0.22 mGal over existing altimeter-derived models. In local coastal and high-latitude regions, SDUST2022GRA showed an enhancement of 0.16-0.24 mGal compared to others models. The spatial resolution of SDUST2022GRA is approximately 20 km in certain regions, slightly superior to others models. The percentage contribution of ICESat-2 to the improvement of gravity anomaly model is 4.3% in low-middle latitude regions by comparing SDUST2022GRA with incorporating ICESat-2 to SDUST2021GRA without ICESat-2, and it is increasing in coastal regions. These assessments suggests that SDUST2022GRA is a reliable global marine gravity anomaly model. The SDUST2022GRA are freely available at the site of https://doi.org/10.5281/zenodo.8337387 (Li et al., 2023).

1 Introduction

Marine gravity is a critical piece of marine environmental information, and accurately recovering marine gravity anomalies is essential for marine geophysics, marine geology, and marine dynamics (Hwang et al. 2014; Sandwell et al. 2014; Bidel et al. 2018; Wang et al. 2020). Since the late 1970s, satellite altimetry has provided global sea surface height (SSH) observations, which are associated with the time-invariant marine geoid. Because of its global coverage and consistent accuracy, satellite altimetry is a vital technique for the recovery of marine gravity anomalies, complementing in-situ gravity measurements (Andersen et al. 1998; Watts et al. 2020; Zhang et al. 2021).

The current method for gravity recovery from altimetry is well-established. Normally, the north-south component and east-west component of deflection of the vertical (DOV) on a regular grid, derived from along-track geoid gradients (GGs), are used to recover marine gravity anomaly model via inverse Vening-Meinesz formula or Laplace's equation (Sandwell and Smith 1997; Hwang et al., 2002). The accumulation of altimeter data and advancements in data processing methods have led to the publication and continual refinement of marine gravity anomaly models (Andersen et al., 2021; Zhu et al., 2020). However, there remains a need to improve the accuracy of the global marine gravity anomaly model to investigate small-scale undersea features and tectonics (Yu et al., 2021; Sandwell et al., 2021).

The recovery of marine gravity anomalies primarily relies on along-track radar altimeter data (Hwang et al. 2006; Andersen et al. 2010; Wu et al. 2019). Due to the north-south inclination of satellite orbit, the precision of the north component of the altimeter-derived DOV model is generally higher than the east component (Che et al., 2021; Jin et al. 2022). The unbalanced accuracy of DOV components severely restricts the improvement of the gravity anomaly model (Hwang 1998, Annan and Wan 2021). New altimeter mode such as twin-satellite altimetry and wide-swath altimetry aim to provide cross-track altimeter data for addressing the unbalanced accuracy (Bao et al. 2013; Yu et al. 2021; Jin et al. 2022). Consequently, incorporating cross-track altimeter data is essential to enhance the marine gravity anomaly model.

Radar altimeter data is a crucial for recovering gravity anomalies, providing centimetre-level accuracy in SSH observations (Vignudelli et al. 2011). Conventional radar altimeter data has a large pulse-limited nadir footprint, spanning a few kilometres in diameter (Escudier et al. 2018). Even with Synthetic Aperture Radar (SAR) altimeter using Doppler shift technology, the pulse-limited footprint is reduced to a few hundred metres only in the along-track direction (Egido and Smith 2016; Vignudelli et al. 2019). The radar echo signal used for SSH observations is susceptible to interference from non-homogeneous reflective surfaces in coastal regions, degrading SSH accuracy and reducing the number of valid SSH observations (Hwang et al. 2006; Escudier et al. 2018). Although altimeter data processing, such as waveform retracking, contributes to improving the quality of SSHs, the precision of gravity anomalies recovered from degraded SSHs in coastal regions is still inferior to that in the open ocean (Passaro et al. 2018; Fernandes et al. 2021). Additionally, few altimetry missions provide altimeter data for regions with latitudes above 66° due to orbital inclination constraints (Li et al. 2022), resulting in degraded gravity anomaly model accuracy

in high-latitude regions (Andersen and Knudsen 2019; Ling et al. 2021). Therefore, incorporating altimeter data with new characteristics is crucial for improving the marine gravity anomaly model, especially in coastal and high-latitude regions.

The ICESat-2 laser altimetry mission (Markus et al. 2017), launched in September 2018, carries the advanced topographic laser altimeter system (ATLAS). ATLAS provides three pairs of laser beams altimeter data, with approximately 3.3 km spacing for each pair in the cross-track direction. This configuration allows for the determination of cross-track height slope (Buzzanga et al. 2021). This provides an opportunity to mitigate the unbalanced accuracy of DOV caused by only using along-track altimeter data. In addition, the ICESat-2 laser beam has a nominal 17 m diameter photon footprint, making SSH observations less susceptible to interference from non-homogeneous reflective surfaces compared to radar altimeter data. Although the small footprint might be adversely affected by surface ocean waves, it is particularly useful for SSH observations in coastal regions (Wang et al. 2022; Wang and Sneeuw 2023). Furthermore, ICESat-2 provides near-global coverage with a 92° inclination, complementing radar altimeter data in high-latitude regions. SSH observations from ICESat-2 have been investigated for applications such as ocean topography recovery, DOV determination, and SSH anomalies variations examination, confirming their quality to be comparable to the best radar altimeter data (Yu et al. 2021; Che et al. 2021; Bagnardi et al. 2021). However, ICESat-2 altimeter data is rarely used in published global marine gravity anomaly models.

The unique characteristics of ICESat-2 laser altimeter data motivates us to develop a new global marine gravity anomaly model and investigate its potential for gravity anomalies recovery. First, we present the ICESat-2 altimeter data processing method for determining cross-track GGs and combining along-track and cross-track altimeter data. The new global marine gravity anomaly model, SDUST2022GRA, is recovered from multi-satellite altimeter data, including radar and laser altimeter data. Second, we assess the accuracy of SDUST2022GRA by comparing published global marine gravity models (NSOAS22, DTU17, V32.1) and shipborne gravity measurements. Finally, we analyse the contribution of ICESat-2 laser altimeter data to the gravity anomalies recovery by comparing SDUST2022GRA with SDUS2021GRA without using ICESat-2 data.

2 Altimeter data and gravity anomalies data

2.1 ICESat-2 laser altimeter data

The ICESat-2 mission provides three pairs of laser beams, each pair consisting of a strong and a weak beam with about 4:1 energy ratio, to measure Earth's surface elevation such as land/sea ice elevation, land/water vegetation elevation, and ocean elevation. For ocean elevation observations, ICESat-2 typically downlinks only strong beam data due to the low surface reflectance. The ICESat-2 product, ocean elevation ATL 12 (level 3, version 5), provides along-track SSHs from three strong beams and is available via NASA's Earth Science Data Systems (EarthData, https://search.earthdata.nasa.gov/).

In ATL12, the SSHs have been corrected for atmospheric delay, dynamic atmospheric errors, tidal errors, sea state bias, and other factors (Morison et al., 2021). The ocean tide correction is derived from the global ocean tide model GOT4.8 with a resolution of 0.5° (Stammer et al., 2012). However, the recent global ocean tide model FES2014 (Carrere et al., 2015), with a

resolution of 0.125°, is used for the L2P product of radar altimeter data. Therefore, the correction from FES2014 instead of GOT4.8 is used for the SSH from ICEsat-2, which is consistent with the product of radar altimeter data. The SSH is referenced to the WGS84 reference ellipsoid (ITRF2014 reference frame, Morison et al., 2021). The ICESat-2 ground track of three strong beams from one cycle (91 days) is shown in Fig. 1. Because of the laser observation dependent on the weather conditions, the along-track ground distance of SSH observations is variable, between 70 m and 7 km.

2.2 Multi-satellites radar altimeter data

The multi-satellites radar altimeter data used in SDUST2022GRA is similar to the previously published SDUST2021GRA (Zhu et al. 2022), which is primarily from altimetry missions after the 1990s. Although the ERS-1 altimeter data makes little contribution to the improvement of the gravity model, the geodetic mission (GM) altimeter data is used for the addition of data coverage, especially in high-latitude regions. In addition, the SAR altimeter data from new missions (Sentinel3A/3B, Sentinel-6A) is also used in SDUST2022GRA. The information about used altimeter data is presented in Table 1. The nominal tracks and interleaved tracks from exact repeat missions (ERM) are labelled "_N" and "_I", respectively.

All SSHs of radar altimeter data were obtained from the non-time critical Level2+ (L2P, version 3) product which was the reprocessing Geophysical Data Records (GDR), except Sentinel-6A. The L2P is available at AVISO (https://www.aviso.altimetry.fr/). The Sentinel-6 SAR altimeter data is from the high-resolution non-time critical ocean surface topography product, which is available at NASA's EarthData (https://search.earthdata.nasa.gov/). All SSHs are from Ku-band altimeter data, except for the SSH of SARAL, which is from Ka-band altimeter data. The SSHs from radar altimeter data both are at 1 Hz sampling frequency and referenced to the WGS84 ellipsoid (CNES 2020).

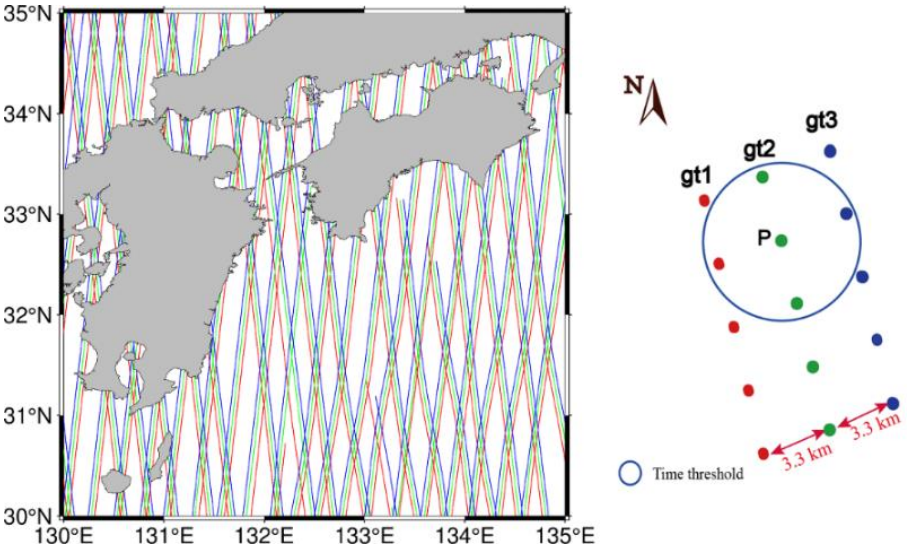

Figure 1 ICESat-2 ground track of three strong beams (cycle_0011)

Table 1 Altimeter data information for global marine field recovery

Altimeter data	Observation Time (Cycles)	Orbit Inclination (°)	Repeat Period (d)	Ground track spacing in equator (km)
ICESat-2	2018.10-2022.04 (001-015)	92	91	30/3/3
SARAL/DP	2016.07-2022.07 (100-162)	98.55	-	5
CryoSat-2/LRM	2010.07-2020.06 (007-130)	92	369	7.5±5
HY-2A/GM	2016.03-2020.06 (118-288)	99.3	168	15
Jason-2/GM	2017.07-2019.10 (500-537/ 600-644)	66	371/350	8.5/4
Jason-1/GM	2012.05-2013.06 (500-537)	66	406	7.5
ERS-1/GM	1994.04-1995.09/1995.09-1995.03 (030-040)	98.52	168	8.3
Sentinel-6A SAR	2020.12-2022.07(004-062)	66	10	293
Sentinel-3A SAR	2016.03-2022.08(001-088)	98.64	27	104
Sentinel-3B SAR	2018.11-2022.07(017-067)	98.64	27	104
SARAL	2013.03-2015.03(001-021)	98.55	35	80
HY-2A	2014.04-2016.03(067-117)	99.3	14	208
HY-2B	2019.12-2022.04(030-090)	99.3		
Jason-3_N	2016.02-2022.04(001-226)			
Jason-2_N	2008.07-2016.10(001-303)			
Jason-2_I	2016.10-2017.05(305-327)			
Jason-1_N	2002.01-2009.01(001-259)	66	10	316
Jason-1_I	2009.02-2012.03(262-374)			
T/P_N	1992.09-2002.08(001-364)			
T/P_I	2002.09-2005.09(369-479)			
Envisat_N	2002.05-2010.10(006-093)	98.55	35	80
Envisat_I	2010.11-2012.04(097-113)			
ERS-2	1995.05-2003.06(001-085)	98.52	35	80
GFO	2001.01-2008.01(037-208)	108	17	165

2.3 Global marine gravity anomaly models

115 The Earth Gravitational Field is typically used as the reference field in the recovery of gravity anomalies in the remove-restore technique. The recently published XGM2019e is a combined global gravity model that combines the satellite gravity model

GOCO06s, the marine gravity anomaly model DTU13, and gravity measurements over land and ocean (Zingerle et al. 2020). Gravity anomalies on a 1′×1′ grid from XGM2019e up to degree and order 2190 are available via the International Centre for Global Earth Models (ICGEM, http://icgem.gfz-potsdam.de/calcgrid), which is used as the reference gravity field for the recovery of SDUST2022GRA.

The recently published global marine gravity anomaly models were obtained to assess the performance of SDUST2022GRA. The commonly recognized global marine gravity anomaly models are the Sandwell and Smith (S&S) series from the Scripps Institution of Oceanography (SIO) and the DTU series from the Technical University of Denmark. The publicly available models include V32.1 of the S&S series (Sandwell et al. 2021) and DTU17 of the DTU series. Additionally, other gravity models were also obtained such as NSOAS22 (Zhang et al. 2022) recovered from incorporating HY-2 altimeter data and the SDUST2021GRA (Zhu et al. 2022) recovered by the improved data fusion method. It is important to note that these models do not yet utilize ICESat-2 laser altimeter data. Table 2 lists the information on global marine gravity anomaly models. According to several studies, the root mean square (RMS) of the difference between altimeter-derived gravity anomaly models and shipborne gravity anomalies is approximately 3-5 mGal (Yu et al. 2022; Wan et al. 2022).

2.4 Shipborne gravity anomalies measurements

Shipborne gravity, as in-situ gravity measurements, are also used to assess the accuracy of gravity anomaly model recovered from altimetry. In general, shipborne gravity anomalies have a higher accuracy and spatial resolution along ship routes compared to altimeter-derived gravity anomaly model. Global shipborne gravity anomalies after the 1990s were obtained from the U.S. National Centers for Environmental Information (NCEI), taking into account the impact of ship navigation on the accuracy of gravity measurements. Gross errors in the shipborne gravity data were removed. First, gravity measurement

Table 2 Global marine gravity anomaly models information

gravity anomaly models	Year	Reference gravity field	Coverage latitudes range	Main altimeter data
DTU17	2019	EGM2008	90°S-90°N	Topex/Poseidon, Jason-1/2/3, ERS-1/2, Envisat, Cryosat-2 (LRM/SAR), SARAL/AltiKa
SIO V32.1	2022	EGM2008	80°S-80°N	Topex/Poseidon, Jason-1/2/3, ERS-2, Envisat, Cryosat-2 (LRM/SAR), SARAL/AltiKa, Sentinel-3A/3B
NSOAS22	2022	EGM2008	80°S-80°N	Geosat, ERS-1, Jason-1/2, Cryosat-2, SARAL/AltiKa, HY-2A/2B/2C/2D
SDUST2021GRA	2022	XGM2019e	80°S-80°N	Topex/Poseidon, Jason-1/2/3, Envisat, Cryosat-2 (LRM), SARAL/AltiKa, HY-2A

cruises with significant error were discarded, and outliers exceeding three times the standard deviation for each cruise were removed by comparison with XGM2019e. Second, system biases in gravity anomalies from each cruise, caused by gravimeter drift, were corrected using a quadratic polynomial (Hwang and Parsons, 1995). After data editing, the remaining shipborne gravity anomalies are 7 012 812 points (486 cruises) with a rejection rate of 2.9%. The distribution of shipborne gravity anomalies is illustrated in Fig. 2.

Since global shipborne gravity anomalies are gathered from various agencies, the NCEI does not give information on the precision of shipborne gravity measurements. The precision of shipborne gravity is verified by the discrepancies of gravity anomalies at crossover points. In the global ocean, the total number of crossover points is 49 277, and the RMS of discrepancies is about 3.99 mGal. The precision of shipborne gravity, about 2.82 mGal, is derived by dividing RMS by the square root of two based on the error propagation law. It is generally consistent with the shipborne gravimeter measurements of 1-3 mGal magnitude (Zaki et al. 2022).

We selected six study regions characterized by SSH variations due to current or undersea features to investigate the recovery of gravity anomalies. These regions include two open ocean regions (A1 and A2), three coastal regions (B1, B2, and B3), and a high-latitude region (C1), as illustrated in Fig. 2. Regions A1 and B1 are located in the Kuroshio Current region, and Region A2 is located in the North Atlantic near the Mid-Atlantic Ridge. Regions B2 and B3 are situated in the Gulf of California and the coastal regions of New Zealand, respectively, respectively. Region C1 is a part of the Southern Ocean, located in the eastern Ross Sea and influenced by the Antarctic Circumpolar Current.

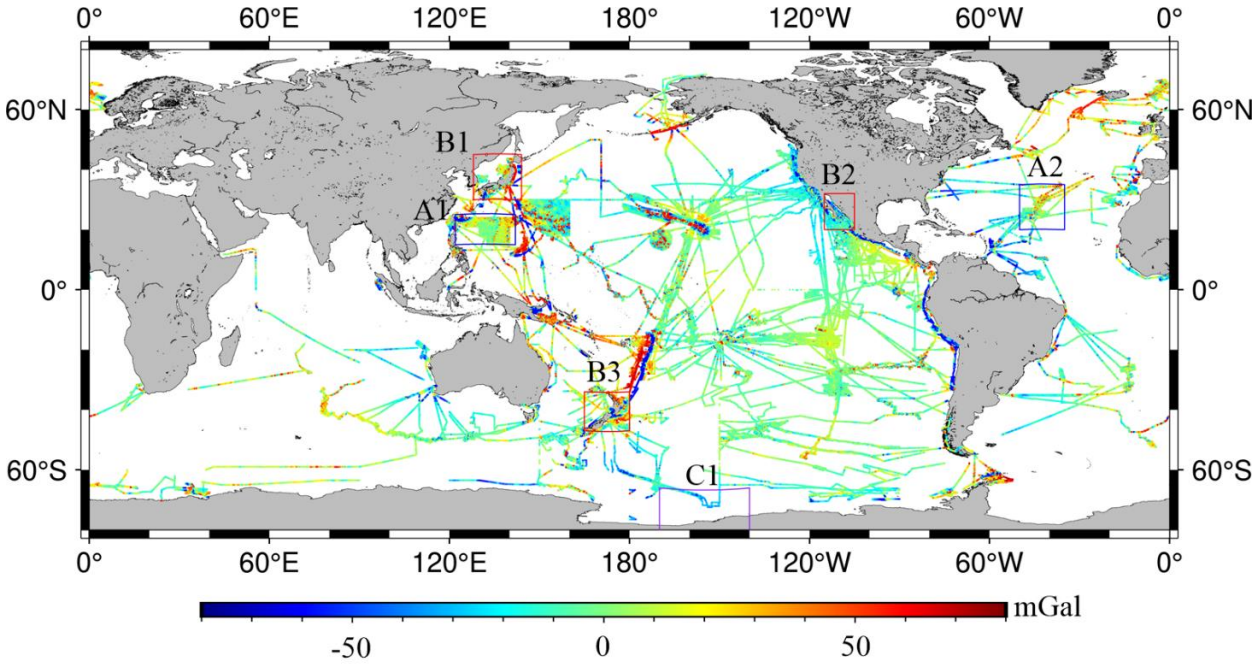

Figure 2 Global available shipborne gravity anomalies from NCEI after the 1990s and local study regions

3 Marine gravity recovery methods

3.1 Multi-satellites radar altimeter data processing

It is a conventional method for the recovery of gravity anomalies from along-track radar altimeter data. First, several errors in SSH observations are corrected, including instrument errors, atmosphere delay, geophysical corrections, etc. For ERM radar altimeter data, a simplified collinear adjustment is used to remove the residual time-variable error (Rap et al. 1994; Yuan et al. 2019). For GM along-track altimeter data, Gaussian filtering is applied to remove the high-frequency error (Zhu et al. 2020). Second, the residual geoid heights are determined by removing the mean dynamic topography model and the reference geoid model from the corrected SSHs. The removed valve of MDT_CNES_CLS18 (Mulet et al. 2021) or geoid model at corresponding position of SSHs is derived by the bivariate spline interpolation. The residual along-track GG is derived by

$$e_{\alpha,res} = \frac{\Delta N_{pt1} - \Delta N_{pt1}}{d_{pt1\_pt2}} \tag{1}$$

where $e_{\alpha,res}$ is the residual GG with azimuth (α) at the central location of points pt1 and pt2, ΔN_{pt1} and ΔN_{pt2} are residual geoid height at pt1 and pt2, respectively. d_{pt1_pt2} is the spherical distance between two points.

The residual GGs can be converted to the north and east components of DOV by using the least-squares collocation (LSC). The LSC is also a method of multi-satellites altimeter data fusion by determining the error variance from each altimeter data. The error variance of GG from each altimeter data can be derived using the error propagation law of Eq. (1) while ignoring the distance error of two points, as

$$m_e^2 = \frac{m_{ssh,pt1}^2 + m_{ssh,pt2}^2}{d_{pt1\_pt2}^2} \tag{2}$$

where m_e is the standard deviation (STD) of GGs to determine the error variance (C_{nn} in LSC) of GGs, $m_{ssh,P}$ and $m_{ssh,Q}$ are the STD of SSH observations at pt1 and pt2, respectively.

The crossover discrepancies of SSH and the iterative method are applied to determine the GG errors from Ku-band and Ka-band altimeter data, respectively. In the crossover adjustment, a residual SSH errors is established using a combination function of a general polynomial and a trigonometric polynomial (Huang et al. (2008) as

$$f(t) = a_0 + a_1(t - t_0) + \sum_{i=1}^{n}\left[C_i \cos(i\omega(t - t_0)) + S_i \sin(i\omega(t - t_0))\right] \tag{3}$$

where $f(t)$ is the SSH correction, t is the observation time, t_0 and t_1 are the beginning and end observation times of each ground track, respectively. ω is the angular frequency ($\omega = 2\pi/(t_1 - t_0)$), a_0, a_1, C_i, and S_i are unknown parameters to be solved by the least-squares method. The integer n is determined based on the number of crossover points.

The iterative method (Zhu et al. 2020) is applied to determining the error of GG from the Ka-band altimeter data (SARAL/DP), which contributes to improving the accuracy of the marine gravity anomaly model. This method depends on the relationship among the error of altimeter-derived gravity, the error of GGs, and the average number of GGs, as

$$D_{\Delta g} = \beta_0 + \beta_1 \frac{\rho}{m_e^2} \tag{4}$$

where $D_{\Delta g}$ is the error variance of altimeter-derived gravity, ρ is the average number of GGs on $1' \times 1'$ grid, unknown parameters β_0 and β_1 can be solved by the least square method based on the error variance of altimeter-derived gravity, the error of GGs, and the average number from each Ku-band altimeter data.

The iterative equation for the error variance solution of GGs is

$$C_{nn}^{e,j+1} = \frac{\rho\beta_1}{D_{\Delta g,j} - \beta_0} \qquad j = 0,1,2\cdots \tag{5}$$

The initial value $D_{\Delta g,0}$ is determined using the gravity anomalies recovered from the initial error of GGs (SARAL/DP) derived by the RMS of crossover discrepancies. The termination condition of the iteration is that the difference between the adjacent error of GG ($C_{nn}^{e,j+1}$ and $C_{nn}^{e,j}$) is less than a threshold (provided in Section 4.2).

3.2 ICESat-2 laser altimeter data processing

The ICESat-2 SSH observations at varying length scales is resampled at 1 Hz for each beam to achieve a uniform distribution of SSHs. In the resampling, SSHs at varying length scales are fitted using a quadratic polynomial in latitude to mitigate the effect of high-frequency noise and outliers. Each 1-s SSHs is used to solve polynomial coefficients and then produced SSHs at the median of the latitude. If the number of observations is less than the minimum required for solving polynomial coefficients, the 1-s SSHs are averaged directly to 1 Hz. The quadratic polynomial function of latitude is (Yu and Hwang, 202)

$$l_i + v_i = a\varphi_i^2 + b\varphi_i + c \tag{6}$$

where l_i is the SSH observation at point i with in a time threshold, v_i is the residual at point i, φ_i is the latitude at point i, and a, b, c are the coefficients of the quadratic polynomial.

The method of determining cross-track GGs is presented using ICESat-2 multiple beam observations. A major difference between the radar altimeter data and ICESat-2 laser altimeter data processing is the determination of cross-track GGs. In Eq. (1) of the last section, the along-track GG is determined from adjacent SSH observations on a single beam. For determining cross-track GGs, it is necessary to select the associated SSHs from different beam observations. Otherwise, a cross-track GG with an azimuth that deviates from the east-west direction may not be able to mitigate the unbalanced accuracy of DOV.

Since three beams of ICESat-2 observations are not exactly simultaneous, the determination of cross-track GG involves the following steps: (1) Select the beam with the maximum number from two-beam altimeter data as the reference altimeter data, (2) Based on the reference beam observations, determine the cross-track GG within a time and azimuth threshold, (3) If there are multiple GGs for each reference observation, use only the cross-track GG with an azimuth closet to perpendicular to the orbit inclination for the recovery of gravity anomalies. A schematic diagram of determining the cross-track gt13 GGs from ICESat-2 altimeter data is shown in Fig. 3. The cross-track GG determination strategy is defined as follows:

$$\begin{cases} \text{Reference\_beam} = \text{Max}[\text{Num}_{\text{gt1}}, \text{Num}_{\text{gt3}}] \\ \left|T_i - T_{ref}\right| \le T\_Threshold \\ \left|\alpha_{GG,i} - \alpha_{ref\_inc}\right| \le A\_Threshold \\ \text{Cross\_track\_GG} = \text{Min}[\alpha_{GG,i} - \alpha_{ref\_inc}] \end{cases} \tag{7}$$

where $\text{Num}_{\text{gt1}}, \text{Num}_{\text{gt2}}$, and Num_{gt3} are the number of each beam observations, respectively. T_{ref} is the observation time of reference beam, T_i is the observation time of the other beam, $\alpha_{GG,i}$ is the azimuth of GG derived from two-beam observations at the number i . α_{ref_inc} is a reference azimuth perpendicular to the orbit inclination. $T\_Threshold$ is a time threshold, and 1 s is selected as time threshold to reduce the effect of random errors, $A\_Threshold$ is an azimuth threshold, $\pi/4$ serves as a azimuth threshold to obtain GGs with azimuth toward east-west direction.

Any two of three tracks from ICESat-2 can be used to determine the cross-track GG, named gt12, gt23, and gt13, respectively. The LSC is employed to fuse along-track and cross-track GGs based on the error variance of GGs. The error variance of cross-track GGs is derived from the error of associated SSHs.

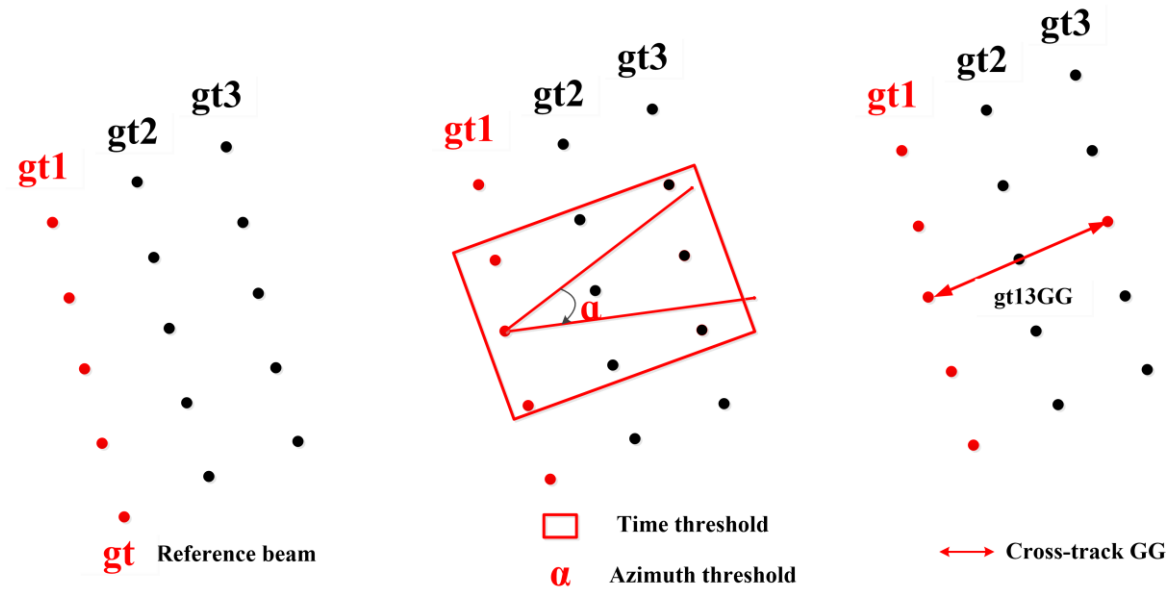

Figure 3 The schematic diagram of determining the cross-track geoid gradients from gt1 and gt3 beams of ICESat-2

3.3 Gravity anomalies recovery method

We determined the DOV components by LSC (Hwang and Parsons, 1995) as

$$\begin{pmatrix} \xi_{res} \\ \eta_{res} \end{pmatrix} = \begin{pmatrix} C_{\xi_e} \\ C_{\eta e} \end{pmatrix} \left(C_{ee} + C_{nn} \right)^{-1} e_{res,\alpha} \tag{8}$$

where ξ and η are the residual north and east component of the DOV, respectively. C_{ξ_e} (or $C_{\eta e}$) is covariance matrix for the north (or east) component of the DOV and GG, C_{ee} is covariance matrix for the GG and GG. The diagonal matrix C_{nn} is the error variance of GGs. $e_{res,\alpha}$ is residual GGs.

The covariance function of residual disturbing potentials at the given distance can be calculated by errors of coefficients in the potential set with Model 4 proposed by Tscherning and Rapp (1974). Because the longitudinal and transverse components are isotropic, the covariance of longitudinal C_{ll} and transverse C_{mm} for GGs can be derived by the covariance function. Therefore, the covariance matrices (C_{ξ_e}, $C_{\eta e}$ and C_{ee}) are obtained by (Hwang and Parsons, 1995)

$$\begin{cases} C_{\xi e} = -C_{ll} \cos\alpha_{PQ} \cos(\alpha_{eQ} - \alpha_{QP}) + C_{mm} \sin\alpha_{PQ} \sin(\alpha_{eQ} - \alpha_{QP}) \\ C_{\eta e} = -C_{ll} \sin\alpha_{PQ} \cos(\alpha_{eQ} - \alpha_{QP}) - C_{mm} \cos\alpha_{PQ} \sin(\alpha_{eQ} - \alpha_{QP}) \\ C_{ee} = C_{ll} \cos(\alpha_{eP} - \alpha_{PQ}) \cos(\alpha_{eQ} - \alpha_{PQ}) + C_{mm} \sin(\alpha_{eP} - \alpha_{PQ}) \sin(\alpha_{eQ} - \alpha_{PQ}) \end{cases} \tag{9}$$

where α_{eP} and α_{eQ} are azimuths of satellite ground track at points P and Q, respectively. α_{PQ} (or α_{QP}) is the azimuth from P to Q (Q to P).

The gravity anomaly model is recovered by the inverse Vening-Meinesz formula as (Hwang, 1998)

$$\Delta g_p = \frac{\gamma_0}{4\pi}\iint_{\sigma} H'(\psi)\left(\xi_q \cos\alpha_{QP} + \eta_q \sin a_{QP}\right) d_{\sigma_q} \tag{10}$$

where γ_0 is the normal gravity. $H'(\psi) = -\frac{\cos\psi/2}{2\sin^2\psi/2} + \frac{\cos\psi/2\,(2\sin\psi/2+3)}{2\sin\psi/2\,(\sin\psi/2+1)}$ is a kernel function of the spherical distance between two points. d_{σ_q} is the areal element of the unit sphere σ.

The gravity anomalies on the innermost-zone is derived by

$$\Delta g_{p,i} = \frac{s_0\gamma_0}{2}(\xi_y + \eta_x) \tag{11}$$

where, ξ_y and η_x are obtained by numerical differentiations of the GGs. $s_0 = \sqrt{\frac{\Delta x \Delta y}{\pi}}$ is the radius of the innermost zone. Δx and Δy are the grid intervals.

4 Gravity anomaly model recovery and assessment

4.1 Gravity anomalies recovered from ICESat-2

For the recovery of gravity anomalies from ICESat-2 altimeter data, SSHs at varying length scales from ICESat-2 are resampled to 1 Hz to integrate them with radar altimeter data. The quality of SSHs and the recovered gravity anomalies from SSHs at different sampling frequency are listed in Table 3. After resampling, the total number of SSHs is reduced, but the RMS of SSHs crossover discrepancies improves by about 0.01 m. Moreover, the RMS of gravity anomalies from SSH at 1 Hz assessed by SIO V32.1 is slightly better than that of SSHs at varying length scales, which assessed by shipborne gravity and SIO V32.1. Consequently, SSHs of ICESat-2 resampled at 1 Hz are used to recover global marine gravity anomalies.

The filtering radius is determined by the accuracy of the recovered gravity anomalies. For resampled SSHs of ICESat-2, the average ground distance of along-track adjacent observations is about 7 km, so the filtering radius with a multiple of 7 km is applied to recover marine gravity anomalies from along-track altimeter data. When the filtering radius is 7 km, the RMS of difference between gravity anomalies recovered from along-track altimeter data and shipborne gravity anomalies is 5.56 mGal. The result is better than that without using Gaussian filtering (5.61 mGal) or with a filtering radius of 14 km (5.58 mGal). Thus, the filtering radius of 7 km is selected for the recovery of gravity anomalies from ICESat-2 along-track SSHs.

Table 3 The quality of ICESat-2 SSHs and gravity models recovered from SSHs at varying length scales and at resampled 1 Hz

SSHs at different sampling frequency	The number of SSHs	The RMS of SSH crossover discrepancies after adjustment (m)	The difference between Gravity anomalies recovered from ICESat-2 and Shipborne gravity (mGal)		The difference between Gravity anomalies recovered from ICESat-2 and SIO V32.1 (mGal)	
			|Max|	RMS	|Max|	RMS
SSHs at varying length scales	1 457 596	0.124	50.02	5.44	52.30	3.06
SSHs at 1 Hz	854 533	0.115	49.54	5.42	52.01	2.89

Table 4 Differences between ICESat-2 altimeter-derived gravity and ship-borne gravity (Unit: mGal)

Gravity anomaly model	Max	Min	Mean	STD	RMS
gt1+gt2+gt3	50.83	-48.28	-0.13	5.56	5.56
gt12+gt1+gt2+gt3	49.35	-48.18	-0.10	5.66	5.66
gt23+gt1+gt2+gt3	54.92	-54.98	-0.06	5.70	5.70
gt12+gt23+gt1+gt2+gt3	47.07	-46.75	-0.07	5.65	5.65
gt13+gt1+gt2+gt3	49.54	-48.05	-0.03	5.42	5.42

Table 5 The number and STD of residual GGs from ICESat-2

Residual GGs	gt1	gt2	gt3	gt12	gt23	gt13
Number	302407	250988	301138	202492	200312	209769
STD(urad)	1.93	1.88	1.91	2.66	2.75	1.94

The combination of along-track and various cross-track GGs was investigated for the recovery of gravity anomalies. Specifically, combinations such as gt1+gt2+gt3+gt12, gt1+gt2+gt3+gt23, gt1+gt2+gt3+gt13, and gt1+gt2+gt3+gt12+gt23 were analysed. Table 4 lists the differences between gravity anomalies recovered from ICESat-2 and shipborne gravity. The RMS of the gravity model recovered from gt1+gt2+gt3+gt13 is 0.14 mGal better than that recovered from gt1+gt2+gt3, indicating that incorporating gt13 cross-track GGs improves the accuracy of gravity anomaly model. However, incorporating gt12 or gt23 cross-track did not significantly enhance the model's accuracy. For this reason, we analyzed the number of observations from three beams, the precision of SSHs and GGs. Table 5 shows the quality (number and standard deviation) of along-track and cross-track GGs, while Table 6 lists the precision of SSHs from three beams. Although the precision of SSHs from the gt2 beam observation is slightly superior to that from the gt1 or gt3, it is not straightforward to determine that the precision of cross-track GGs. The precision of GG depends not only on the precision of SSHs but also to the distance between the two points. The STD of gt13 GGs is closer to that of along-track GGs than gt12 and gt23. Furthermore, the number of gt2

beam observation is less than gt1 or gt3 beam observations, resulting in the number of gt13 cross-track GGs being more than that other cases. Therefore, the combination of along-track and gt13 cross-track GGs was used to recover marine gravity anomalies.

4.2 Global gravity anomalies recovered from all altimeter data

The GG error from each altimeter data is determined using SSH crossover discrepancies to fuse multi-satellites altimeter data, excluding SDRAL/DP altimeter data. Crossover discrepancies are determined based on the time interval between ascending and descending track observations. These discrepancies are computed from SSH observations collected within the smallest sub-cycle (approximately 30 days) of each altimetry missions, accounting for the number of crossover points and sea surface variation. For each ERM altimeter data, the crossover discrepancies are obtained from SSHs after collinear adjustment without the limit of time. The RMS of SSH crossover discrepancies is detailed in Table 6.

The GG error of SARAL/DP altimeter data is determined by the iterative method. Unknown parameters (β_0 and β_1) in iterative equation (Eq. 5) are solved through a least squares approach, considering the gravity anomaly model error, the GG error, and the average number within a 1′×1′ grid from each Ku-band GM altimeter data, as shown in Table 7. Specifically, the parameter β_0 is found to be 8.96 and the β_1 is -11.84 ($R^2 = 0.98, \mathrm{RMS} = 0.04$). The GG errors determined by crossover discrepancies and the iterative method are shown in Table 8. Based on the GG error of SARAL/DP determined by the iterative method, the accuracy of gravity anomalies recovered from SARAL/DP shows an improvement of 9.1% compared to the result of crossover discrepancies. Therefore, the GGs error variance of 2.37 is used for SARAL/DP altimeter data.

The accuracy and execution time of gravity anomalies recovery are impacted by the window length of LSC, which is connected to the amount of altimeter data. When the window length is 0.2°, the recovery of gravity anomalies is balanced between accuracy and execution time, as shown in Table 9. The global ocean region (0°E-360°E, 80°S-82°N) is divided into 144 (18×8, longitude by latitude) sub-regions for the recovery of the global marine gravity anomaly model, and each sub-region is extended outward 1° to mitigate boundary difference of gravity anomalies. The new global marine gravity anomaly model SDUST2022GRA (free air) on a 1′×1′ grid is recovered from multi-satellites altimeter data, as shown in Fig. 4.

Table 6 The RMS of SSH crossover discrepancies

Altimetry	Satellite Mission	Average along-track ground distance (km)	Crossover discrepancies (30 d)	
			RMS before adjustment (m)	RMS after adjustment (m)
Laser altimetry	ICESat-2/gt1	7.1	0.131	0.117
	ICESat-2/gt2	7.1	0.128	0.109
	ICESat-2/gt3	7.1	0.138	0.119

GM (Radar altimetry)	SARAL/DP	7.0	0.110	0.085
	Cryosat-2	6.4	0.082	0.060
	H2A	6.5	0.103	0.076
	J2	5.8	0.114	0.088
	J1	5.8	0.108	0.079
	E1	6.4	0.117	0.097
ERM (Radar altimetry)	Sentinel-6A SAR	5.8	0.022	0.013
	Sentinel-3A SAR	6.7	0.027	0.018
	Sentinel-3B SAR	6.7	0.035	0.026
	SARAL	7.0	0.034	0.020
	HY-2A	6.5	0.030	0.020
	HY-2B	6.5	0.032	0.024
	T/P-Jason_A	5.9	0.027	0.018
	T/P-Jason_B	5.9	0.026	0.019
	Envisat_A	7.5	0.033	0.022
	Envisat_B	7.5	0.042	0.024
	ERS-2	6.6	0.040	0.034
	GFO	6.7	0.034	0.019

Table 7 Altimeter gravity error, geoid heights error, and average number of geoid heights from Ku-band altimeter data

Gravity anomaly model	STD of difference between altimeter-gravity and shipborne gravity (mGal)	STD of difference between altimeter-gravity and SIO V32.1 (mGal)	Error variance of altimeter-gravity ($mGal^2$)	Error variance of GGs ($mGal^2$)	Geoid gradient average number
Jason-1/GM-derived	5.59	3.09	9.00	7.84	0.146
Jason-2/GM-derived	5.53	3.11	8.70	9.86	0.229
HY-2A/GM-derived	5.42	2.97	7.67	5.81	0.465
Cryosat-2-derived	5.08	2.78	5.29	3.72	1.177

300 **Table 8 Marine gravity anomaly recovered from Ka-band altimeter data by different error of geoid gradients**

Method	Error variance of GGs (mGal^2)	STD of difference between altimeter-gravity and shipborne gravity (mGal)	STD from altimeter-gravity and SIO V32.1 (mGal)	STD of altimeter-gravity error (mGal)
The crossover discrepancies method	6.35	5.19	2.77	2.42
The iterative method	2.37	5.00	2.75	2.20

Table 9 The accuracy and execution time of gravity anomalies recovered by different window lengths in a sub-region (21°×21°)

Window length(°)	0.1	0.2	0.3	0.4
RMS(mGal)	4.71	4.56	4.55	4.55
Time(s)	5530	141232	485218	1418156

Time was calculated based on CPU AMD Ryzen 5-3500X 6-Core @ 3.60GHz

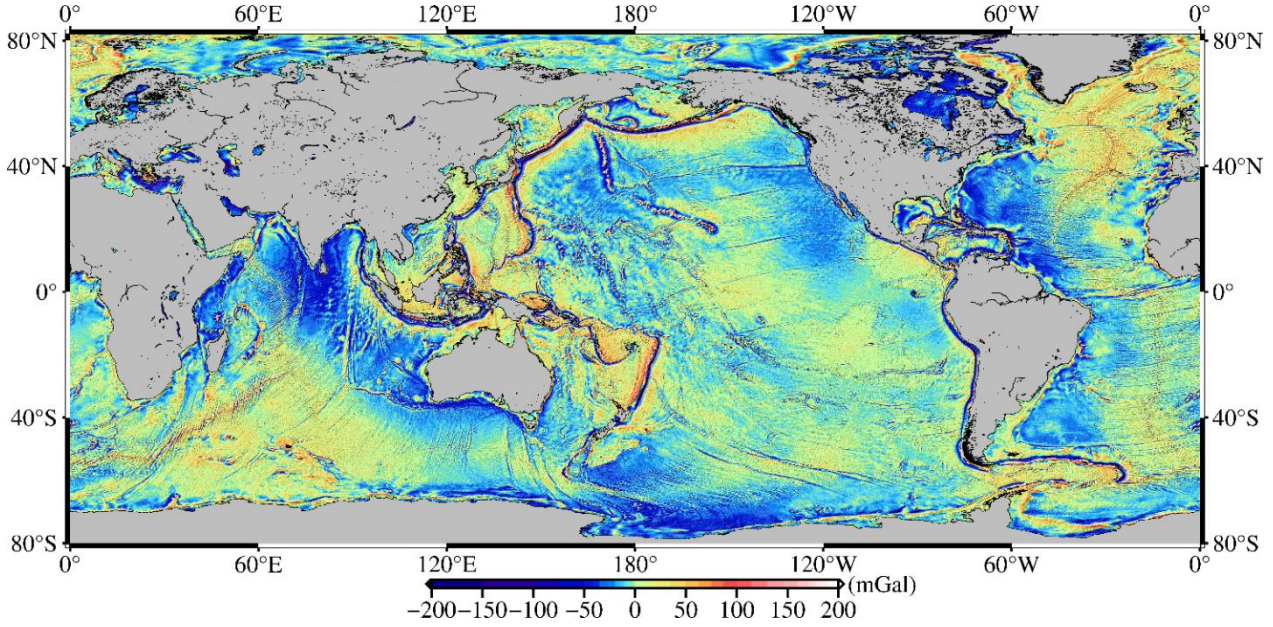

Figure 4 The global marine gravity anomaly model SDUST2022GRA (free air) recovered from radar and laser altimeter data

4.3 Assessment of gravity anomaly model accuracy

The accuracy of SDUST2022GRA is evaluated using shipborne gravity anomalies in both global and local ocean regions. The differences between global gravity anomaly models and global shipborne gravity anomalies are listed in Table 10. Among four global gravity anomaly models, the precision of SDUST2022GRA and SIO V32.1 is generally better than that of NSOAS22

and DTU17, which primarily benefiting from the addition of new altimeter data. In low-middle latitude regions, the precision of SDUST2022GRA is 4.43 mGal, representing an improvement of 0.22 mGal over SIO V32.1. Additionally, the precision of all gravity anomaly models in low-middle latitude regions is significantly better than that in high-latitude regions. The main reason for the degraded accuracy of gravity model in high-latitude regions is the reduction of altimeter data (see Fig. 8).

The precision of gravity anomaly models is further analysed across different local regions, including open ocean regions (A1 and A2), local coastal regions (B1, B2, and B3), and high-latitude region (C1). The mean and RMS differences between gravity anomaly models and shipborne gravity anomalies in these regions are presented in Table 11. Notably, shipborne gravity within 20 km of coastline are used to assess gravity anomaly model in coastal regions.

The precision of all gravity models in open ocean regions is significantly better than that of gravity models in coastal and high-latitude regions. This shows that degraded SSH can significantly reduce the precision of gravity anomalies, especially in coastal regions and high-latitude regions. In local open ocean regions, SIO V32.1 and SDUST2022GRA each have their own advantages resulting from unique improvement methods and the addition of altimeter data. For instance, SIO V32.1 benefits from the improvement of along-track SSH gradients derived by two-pass waveform retracking, while SDUST2022GRA gains from the fusion of along-track and cross-track GGs from multi-satellites altimeter data. In local coastal and high-latitude regions, the RMS of the SDUST2022GRA is 0.16-0.24 mGal better than that of SIO V32.1, which primarily benefiting from the valid observations from ICESat-2 laser beam. This assessment suggests that SDUST2022GRA achieves a higher accuracy than other models in coastal regions. Thus, SDUST2022GRA recovered by incorporating ICESat-2 laser altimeter data is a reliable global marine gravity anomaly model.

Table 10 The difference between gravity anomaly models and global shipborne gravity (Unit: mGal)

Region	Model	Max	Min	Mean	STD	RMS
Global ocean [80°S, 82°N]	NSOAS22	99.46	-81.17	-0.10	5.73	5.73
	DTU17	99.25	-71.85	-0.13	5.42	5.42
	SIO V32.1	77.17	-86.24	-0.10	5.18	5.18
	SDUST2022GRA	96.79	-68.51	-0.08	5.07	5.07
Low-middle latitude regions [60°S, 60°N]	NSOAS22	78.04	-81.17	-0.07	5.26	5.26
	DTU17	78.44	-71.85	-0.12	4.89	4.89
	SIO V32.1	76.25	-86.23	-0.06	4.65	4.65
	SDUST2022GRA	64.44	-67.00	-0.09	4.43	4.43
High-latitude regions [80°S, 60°S)& (60°N, 82°N]	NSOAS22	99.46	-70.56	-0.47	9.76	9.77
	DTU17	99.25	-68.48	-0.25	9.82	9.82
	SIO V32.1	77.17	-76.54	-0.51	9.53	9.54
	SDUST2022GRA	96.79	-68.48	-0.26	9.69	9.69

Table 11 The Mean and RMS of difference between gravity anomaly models and shipborne gravity in local regions (Unit: mGal)

Local region		NSOAS22		DTU17		SIO V32.1		SDUST2022GRA	
		Mean	RMS	Mean	RMS	Mean	RMS	Mean	RMS
Region A1	Open ocean	0.15	3.58	0.10	3.24	-0.10	3.15	0.20	3.04
Region A2		-0.41	5.13	-0.41	4.29	0.14	3.78	0.01	4.01
Region B1	Coastal region	-1.51	8.47	-1.81	7.21	0.10	6.25	-0.16	6.08
Region B2		-0.86	10.66	-1.41	10.33	-0.56	7.85	-0.57	7.69
Region B3		0.10	12.12	-1.24	11.25	-0.67	10.32	-0.68	10.10
Region C1	High-latitude region	0.33	5.86	0.15	5.36	0.12	5.38	0.12	5.14

4.4 Assessment of gravity anomaly model resolution

The spatial resolution of the gravity anomaly model in a local region is generally determined by spectral coherence analysis along shipborne gravity measurements tracks (Marks et al. 2016). The wavelength corresponding to a coherence magnitude squared (CMS) value of 0.5 is considered the highest spatial resolution of a gravity anomaly model. We used shipborne gravity anomalies from three cruises to determine the spatial resolution of SDUST2022GRA, SIO V32.1, and DTU17, as shown in Fig. 5. The CMS between gravity anomaly models and shipborne gravity is presented in Fig. 6.

The wavelengths corresponding to a CMS value of 0.5 for SDUST2022GRA are 18.6 km in a local open ocean region, 20.7 km in high latitude region, and 20.4 km in a coastal region, respectively. The spatial resolution of SDUST2022GRA in the open ocean is generally superior to that in high latitude and coastal regions, which is largely related to the density of the altimeter data. The average number of altimeter data within a 1′×1′ grid in the open ocean is significantly higher than in high latitude and coastal regions (see Fig. 8). The spatial resolution of the SDUST2022GRA is approximately 20 km in a certain region, which is slightly better than that of DTU17 and SIO V32.1. Although SDUST2022GRA incorporates ICESat-2 altimeter data, the resolution is not significantly increased compared to DTU17 and SIO V32.1. Therefore, it is still a challenge to achieve a gravity anomaly model with a spatial resolution of a few kilometres from current altimeter data, and anticipation for the future wide-swath altimeter data from the SWOT altimetry mission (launch on 16/12/2022).

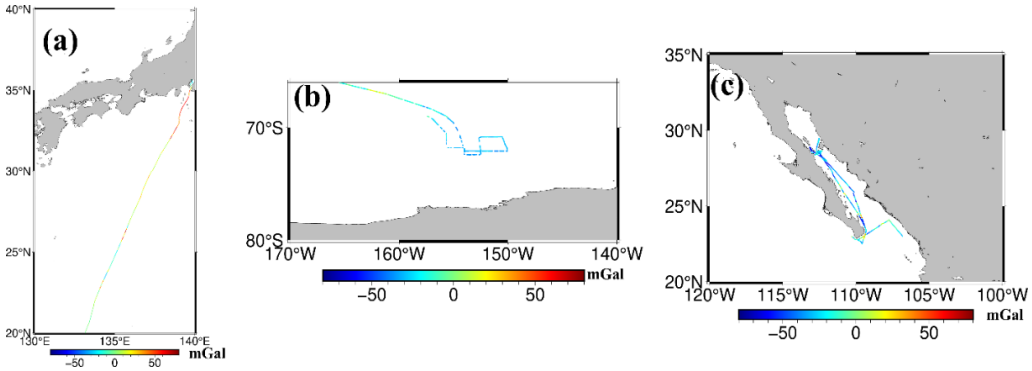

Figure 5 Shipborne gravity (used to determine CMS) of different cruises. a: the jare33l1 with average distance interval of 0.45 km. b:. the ew9201 with average distance interval of 0.80 km. c: the moce05mv with average distance interval of 0.22 km.

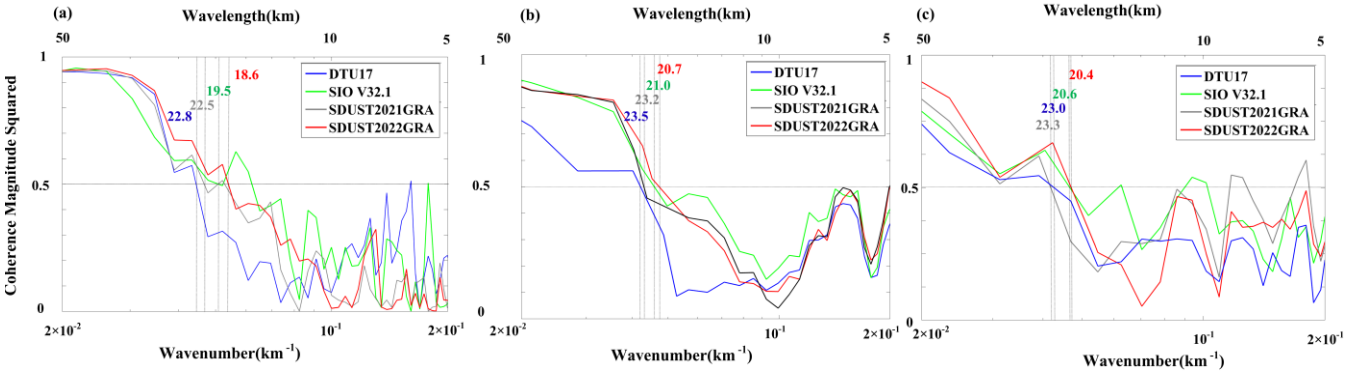

Figure 6 The CMS between the gravity model and shipborne gravity of different cruises: (a) jare33l1, (b) ew9201, (c) moce05mv.

5 Assessment of ICESat-2 contribution

5.1 Contribution on model accuracy

The contribution of ICESat-2 to the improvement of the gravity anomaly model is investigated in precision and spatial resolution. It is widely recognized that GM radar altimeter data play an important role in the recovery of marine gravity anomalies. The role of ICESat-2 in the ranking of GM altimeter data is also determined according to the gravity anomaly model recovered by removing each GM altimeter data from all altimeter data in the local region (120°E -140°E, 20°N-40°N). The RMS differences between each gravity anomaly model and shipborne gravity anomalies are listed in Table 12. The results demonstrate that the SARAL/DP and Cryosat-2 altimeter data provide a major improvement in the accuracy of the gravity anomaly model. Notably, the contribution of ICESat-2 to the improvement outperforms that of other GM altimeter data. This indicates that ICESat-2 altimeter data is on par with most GM altimeter data and is an extremely important dataset for improving marine gravity anomaly model. Additionlly, all ERM data is essential for enhancing the global marine gravity anomaly model.

The contribution of ICESat-2 to the improvement in the accuracy of gravity anomalies is determined by comparing SDUST2022GRA, which incorporates ICESat-2, with SDUST2021GRA, which does not. Although the ICESat-2 altimeter data is not utilized in DTU17 or SIO V32.1, the difference between the SDUST2022GRA and SIO V32.1 (or DTU17) also reflect variations caused by different methods. Given that the SAR altimeter data from S3A/3B and S6A, with sparse coverage are included in SDUST2022GRA, we initially determine the improvement in the precision of gravity anomaly model. The RMS difference between the gravity anomaly model only incorporating SAR altimeter data and shipborne gravity anomalies is 4.64 mGal, consistent with the RMS of SDUST2021GRA without SAR altimeter data. This indicates that SAR altimeter data contributes minimally to the improvement of the gravity anomaly model. Therefore, the difference between SDUST2022GRA and SDUST2021GRA can be attributed primarily to the addition of ICESat-2 altimeter data.

The percentage contribution of ICESat-2 to the improvement of the gravity anomaly model is defined as $\frac{RMS_{\text{SDUST2022GRA}} - RMS_{\text{SDUST2021GRA}}}{RMS_{\text{SDUST2022GRA}}} \times 100\%$, representing the ratio of the improvement of the gravity model recovered by incorporating ICESat-2 to the improvement of the gravity model recovered from all altimeter data, as shown in Table 13. The percentage contribution of ICESat-2 is approximately 2.3% in global ocean regions, while the number of SSH from ICESat-2 takes up 10% of all radar altimeter data. The percentage contribution is 4.3% in low-middle latitude regions, indicating that the ICESat-2 altimeter data contributes to the improvement of the gravity anomaly model recovered from current radar altimeter data.

The percentage contribution of ICESat-2 is also determined in various local regions, including the open ocean, coastal, and high-latitude regions. The difference between SDUST2022GRA and SDUST2021GRA is shown in Fig. 7. The RMS differences between both models are 0.83 mGal and 0.72 mGal in local open ocean regions A1 and A2, respectively. In coastal regions, note that the RMS is only derived from the difference within 20 km of the coastline. They are 1.29 mGal, 0.98 mGal, and 1.26 mGal in local coastal regions B1, B2, and B3, respectively. The RMS is 1.22 mGal in the local high latitude region C1. These results indicate that the variation in the precision of the gravity model is visible by incorporating ICESat-2 altimeter data, especially in coastal and high-latitude regions.

The percentage contribution of ICESat-2 in local coastal and high-latitude regions is generally higher than that in open ocean regions, as shown in Table 14. To investigate the reason for this variation, the average number of GGs from all altimeter data within a 1′×1′ grid is calculated, as presented in Fig. 8. The average number of all radar altimeter data is relatively low in high-latitude and coastal regions, increasing by 50% and 58%, respectively. In open ocean regions, however, it only increasing by 21%, which is lower than that in high-latitude and coastal regions. This suggests that the high percentage contribution of ICESat-2 to the improvement is correlated with the increased proportion of altimeter. In addition, 42% and 35% of the ICESat-2 altimeter data are located in a 1′×1′grid where no radar altimeter data is available in high latitude and coastal regions. In contrast, only 9% of the ICESat-2 is located in a 1′×1′ grid in open ocean region. This indicates that ICESat-2 altimeter data provides complementary SSH coverage due to the reduction of radar altimeter data in high latitude and coastal regions.

Table 12 Ranking of altimeter data contribution to gravity anomaly model recovery

Removed altimeter data	SARAL/ DP	Cryosat-2	ICESat-2	All ERM	HY-2A/ GM	Jason-2/ GM	Jason-1/ GM	ERS-1/ GM	No
RMS (mGal)	4.70	4.66	4.64	4.64	4.61	4.60	4.59	4.57	4.57
RMS difference (mGal)	0.13	0.09	0.07	0.07	0.04	0.03	0.02	0	-

Table 13 The percentage contribution of ICESat-2 altimeter data in global ocean region

Region	$RMS_{SDUST2021GRA}$ (mGal)	$RMS_{SDUST2022GRA}$ (mGal)	△RMS (mGal)	Percentage Contribution
Global ocean	5.19	5.07	0.12	2.3%
Low-middle latitude regions	4.63	4.43	0.20	4.3%
High-latitude regions	9.73	9.69	0.04	0.4%

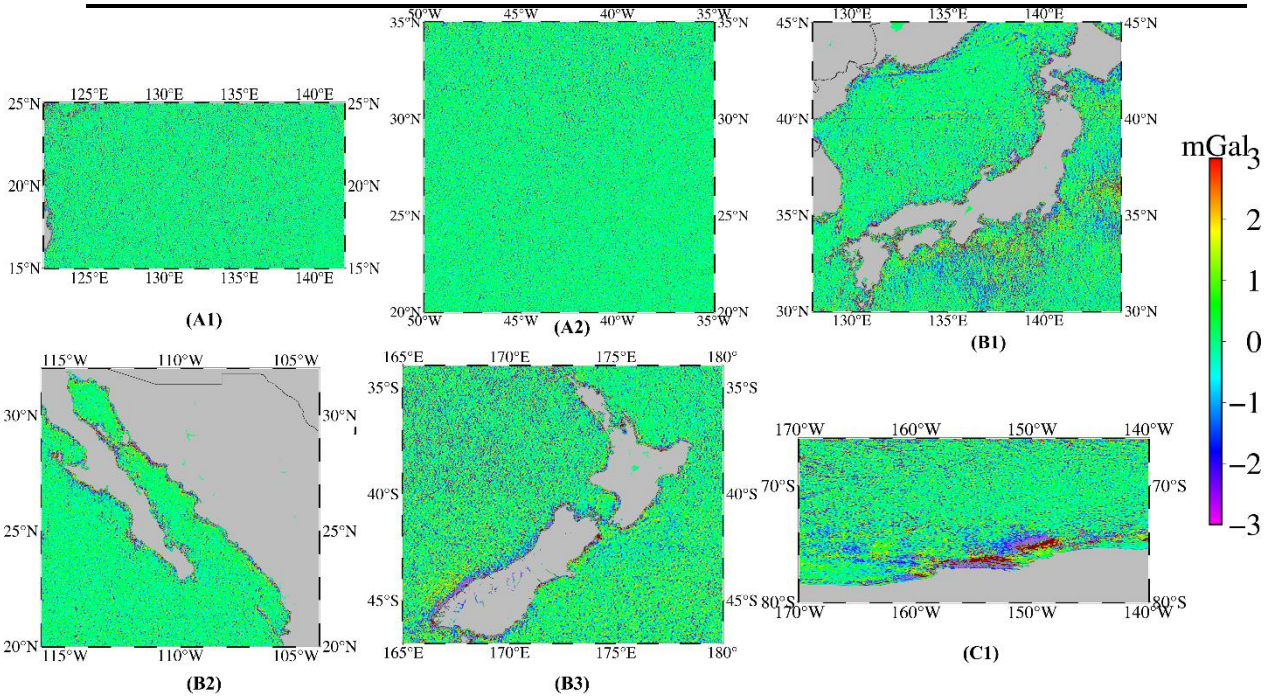

Figure 7 The difference between SDUST2022GRA and SDUST2021GRA in different local regions.

Table 14 The percentage contribution of ICESat-2 altimeter data in different local regions

Local region	$RMS_{SDUST2021GRA}$ (mGal)	$RMS_{SDUST2022GRA}$ (mGal)	△RMS (mGal)	Percentage Contribution
Region A1	3.12	3.04	0.08	2.5%
Region A2	4.07	4.01	0.06	1.5%
Region B1	6.40	6.08	0.32	5.0%
Region B2	7.98	7.69	0.28	3.5%
Region B3	10.51	10.10	0.41	3.9%
Region C1	5.32	5.14	0.18	3.3%

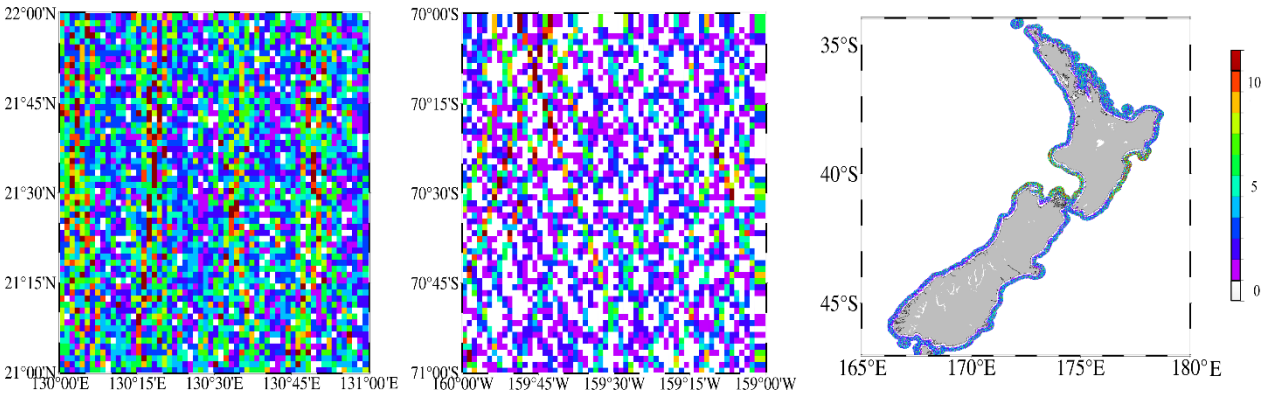

Figure 8 The number of SSHs within the 1′×1′ grid in different local regions. a: open ocean with average number of 3.5. b: the high latitude region with average number of 2.1. c: coastal region with average number of 1.9.

5.2 Contribution on model resolution

To analyze the contribution of ICESat-2 to the spatial resolution of gravity anomaly model, we also compared the spatial resolution of SDUST2022GRA and the SDUST2021GRA, as shown in Fig. 6. The wavelength corresponding to the CMS of 0.5 is reduced from 22.5 km to 18.6 km in the local open ocean, from 23.2 km to 20.7 km in the local high-latitude region, and from 23.3 km to 20.4 km in the local coastal regions, respectively. The spatial resolution of the gravity anomaly model is slightly increased by incorporating the ICESat-2 in a certain local region. However, the increased signal of gravity anomaly is mainly from the power at wavelength greater than 18 km. This suggests that the SSHs of ICESat-2 can improve the marine gravity anomaly model at wavelength >18 km, but the contribution to higher resolution should be small.

6 Data availability

The global marine gravity anomaly model, SDUST2022GRA, is available at the ZENODO repository, https://doi.org/10.5281/zenodo.8337387 (Li et al., 2023). The dataset includes global marine free-air gravity anomalies (WGS84 ellipsoid) in NetCDF file format (i.e., vector of latitudes, vector of longitudes, and matrix of gravity anomalies).

7 Conclusions

The recovery of the global marine gravity anomaly model primarily relies on along-track radar altimeter data. The advanced ICESat-2 laser altimetry mission, which provides SSHs from multiple beams and valid observations in high latitude and coastal regions, offers the potential to mitigate unbalanced accuracy caused by traditional along-track altimeter data and increase altimeter data availability these challenging regions. A novel method for recovering gravity anomalies from cross-track altimeter data is proposed and utilized with ICESat-2 observations. The new global marine gravity model, SDUST2022GRA, is recovered from a combination of along-track and cross-track GGs from multi-satellites altimeter data. According to the recovered SDUST2022GRA and previously published SDUST2021GRA without ICESat-2, we investigate the contribution of ICESat-2 to the recovery of global marine gravity anomaly model, including the combination of along-track and cross-track altimeter data, as well as the addition of SSHs in high latitude and coastal regions.

The precision of SDUST2022GRA is assessed using global shipborne gravity anomalies and published global marine gravity anomaly models (NSOAS22, DTU17, and SIO V32.1). The precision of SDUST2022GRA is 4.43 mGal in low-middle regions, an improvement of at least 0.22 mGal over other published gravity anomaly models. Additionally, SDUST2022GRA exhibits an improvement of 0.16-0.24 mGal in local coastal and high-latitude regions. Spectral coherence analysis reveals that SDUST2022GRA achieves a spatial resolution of approximately 20 km in certain region, which is slightly better than the resolution of DTU17 and SIO V32.1. These indicate that SDUST2022GRA is a reliable global marine gravity anomaly model.

The recovery of gravity anomalies solely from ICESat-2 demonstrates that incorporating cross-track altimeter data improves the precision of gravity anomalies from along-track altimeter data as envisaged. The combination of along-track and cross-track altimeter data from ICESat-2 plays an important role in the recovery of gravity anomalies and can be considered an important dataset following the SARAL/DP and Cryosat-2 altimeter data. By comparing SDUST2022GRA and previous version SDUST2021GRA without ICESat-2, the percentage contribution of ICESat-2 to the improvement of gravity anomaly model is found to be 4.3% in low-middle latitude regions, with a high percentage in coastal regions due to an increased proportion of altimeter data. Therefore, ICESat-2 altimeter data is effective in improving the spatial resolution of gravity anomaly model greater than 20 km, which is similar to the best radar altimeter data.

Author contribution. All authors contributed to recover global marine gravity anomaly model and editing the manuscript.

Competing interests. All authors have no competing interests to declare that are relevant to the content of this article.

Acknowledgments. We are very grateful to NASA's Earth Science Data Systems and AVISO for providing altimeter data, and NCEI for providing global shipborne gravity measurements.

Financial support. This work was partially supported by the National Natural Science Foundation of China (grants 42192535, 42274006, 42242015)

References

Andersen, O.B., and Knudsen, P.: Global marine gravity field from the ERS-1 and Geosat geodetic mission altimetry, J. Geophys. Res., 103(C4), 8129-8137, https://doi.org/10.1029/97JC02198, 1998.

Andersen, O.B., and Knudsen, P.: The DTU17 global marine gravity field: first validation results, In: Mertikas, S., Pail, R. (eds) Fiducial Reference Measurements for Altimetry. Int. Assoc. Geod. Symp. 150. Springer, Cham, pp 83-87, https://doi.org/10.1007/1345_2019_65, 2019.

Andersen, O.B., Knudsen, P., and Berry, P.A.: The DNSC08GRA global marine gravity field from double retracked satellite altimetry, J. Geodesy, 84(3), 191-199, https://doi.org/10.1007/s00190-009-0355-9, 2010.

Andersen, O.B., Zhang, S., Sandwell, D.T., Dibarboure, G., Smith, W. H. F., and Abulaitijiang, A.: The unique role of the Jason geodetic missions for high-resolution gravity field and mean sea surface modelling, Remote Sens., 13, 646. https://doi.org/10.3390/rs13040646, 2021.

Annan, R.F., and Wan, X.: Recovering marine gravity over the Gulf of Guinea from multi-satellite sea surface heights, Front. Earth Sci., 9, 700873, https://doi.org/10.3389/feart.2021.700873, 2021.

Bagnardi, M., Kurtz, N.T., Petty, A.A., and Kwok, R.: Sea surface height anomalies of the Arctic Ocean from ICESat-2: a first examination and comparisons with CryoSat-2, Geophys. Res. Lett., 48(14), e2021GL093155. https://doi.org/10.1029/2021GL093155, 2021.

Bao, L., Xu, H., and Li, Z.: Towards a 1 mGal accuracy and 1 min resolution altimetry gravity field, J. Geodesy, 87(10), 961-969. https://doi.org/10.1007/s00190-013-0660-1, 2013.

Bidel, Y., Zahzam, N., Blanchard, C., Bonnin, A., Cadoret, M., Bresson, A., Rouxel, D., and Lequentrec-Lalancette, M.F.: Absolute marine gravimetry with matter-wave interferometry, Nat. Commun., 9, 627, https://doi.org/10.1038/s41467-018-03040-2, 2018.

Buzzanga, B., Heijkoop, E., Hamlington, B.D., Nerem, R.S., Gardner, A.: An assessment of regional ICESat-2 sea-level trends, Geophys. Res. Lett., 48(9), e2020GL092327, https://doi.org/10.1029/2020GL092327, 2021.

Carrere, L., Lyard, F., Cancet, M., Guillot, A., Picot, N., and Dupuy, S.: FES2014: a new global tidal model. Presented at the Ocean Surface Topography Science Team meeting, Reston. Description at https://datastore.cls.fr/catalogues/fes2014-tide-model, 2015.

Che, D., Li, H., Zhang, S., and Ma, B.: Calculation of deflection of vertical and gravity anomalies over the South China Sea derived from ICESat-2 data, Front. Earth Sci., 9, 670256, https://doi.org/10.3389/feart.2021.670256, 2021.

CNES. Along-track level-2 + (L2P) SLA product handbook. SALP-MU-P-EA-23150-CLS, Issue 2.0. https://www.aviso.altimetry.fr/fileadmin/documents/data/tools/hdbkL2P_all_missions_except_S3.pdf. Assessed 3 November 2022.

Egido, A., and Smith, W.H.: Fully focused SAR altimetry: Theory and applications, IEEE Trans. Geosci. Remote Sens., 55(1), 392-406, https://doi.org/10.1109/TGRS.2016.2607122, 2016.

Escudier, P., Couhert, A., Mercier, F., Mallet, A., Thibaut, P., Tran, N., Amarouche, L., Picard, B., Carrere, L., and Dibarboure, G.: Satellite radar altimetry: Principle, accuracy, and precision, In: Stammer, D., Cazenave, A. (eds) Satellite Altimetry over Oceans and Land Surfaces, CRC Press, Taylor and Francis Group, Boca Raton, FL, USA: New York, NY, USA; London, UK; pp 1–62, 2018.

Fernandes, M.J., Lázaro, C., and Vieira, T.: On the role of the troposphere in satellite altimetry, Remote Sens. Environ., 252, 112149, https://doi.org/10.1016/j.rse.2020.112149, 2021.

Huang, M., Zhai, G., Ouyang, Y., Lu, X., Liu, C., and Wang, R.: Integrated data processing for multi-satellite missions and recovery of the marine gravity field, TAO: Terrestrial, Atmosphere and Ocean Sci., 19(1-2), 103-109, https://doi.org/10.3319/TAO.2008.19.1-2.103(SA), 2008.

Hwang, C.: Inverse Vening Meinesz formula and deflection-geoid formula: applications to the predictions of gravity and geoid over the South China Sea, J. Geodesy, 72(5), 304-312, https://doi.org/10.1007/s001900050169, 1998.

Hwang, C., and Chang, E.T.Y.: Seafloor secrets revealed, Science, 346, 32-33, https://doi.org/10.1126/science.1260459, 2014.

Hwang, C., Guo, J., Deng, X., Hsu, H.Y., and Liu, Y.: Coastal gravity anomalies from retracked Geosat/GM altimetry: improvement, limitation and the role of airborne gravity data, J. Geodesy, 80(4), 204-216, https://doi.org/10.1007/s00190-006-0052-x, 2006.

Hwang, C., Kao, E.C., and Parsons, B.: Global derivation of marine gravity anomalies from Seasat, Geosat, ERS-1 and TOPEX/POSEIDON altimeter data, Geophys. J. Int., 134(2), 449-459, https://doi.org/10.1111/j.1365-246X.1998.tb07139.x, 1998.

Hwang, C., and Parsons, B.: Gravity anomalies derived from Seasat, Geosat, ERS-1 and TOPEX/POSEIDON altimetry and ship gravity: a case study over the Reykjanes Ridge, Geophys. J. Int., 122(2), 551-568, https://doi.org/10.1111/j.1365-246X.1995.tb07013.x, 1995.

Hwang, C.W., Hsu, H.Y., and Jang, R.J.: Global mean sea surface and marine gravity anomaly from multi-satellite altimetry: applications of deflection-geoid and inverse Vening Meinesz formulae, J. Geodesy, 76, 407-418, https://doi.org/10.1007/s00190-002-0265-6, 2002.

Li, Z., Guo, J., Ji, B., and Zhang, S.: A review of marine gravity field recovery from satellite altimetry, Remote Sens., 14(19), 4790, https://doi.org/10.3390/rs14194790, 2022.

Li, Z., Guo, J., Zhu, C., Liu, X., Hwang, C., Lebedev, S., Chang, X., Soloviev, A., and Sun, H.: The global marine free air gravity anomaly model SDUST2022GRA [Data set], Zenodo. https://doi.org/10.5281/zenodo.8337387, 2023.

Ling, Z., Zhao, L., Zhang, T., Zhai, G., and Yang, F.: Comparison of marine gravity measurements from shipborne and satellite altimetry in the Arctic Ocean, Remote Sens., 14, 41, https://doi.org/10.3390/rs14010041, 2021.

Marks, K.M., and Smith, W.H.F.: Detecting small seamounts in AltiKa repeat cycle data, Marine Geophys. Res., 37(4), 349-359, https://doi.org/10.1007/s11001-016-9293-0, 2016.

Markus, T., Neumann, T. Martino, A., Abdalati, W., Brunt, K., Csatho, B., and Zwally, J.: The Ice, Cloud, and Land Elevation Satellite-2 (ICESat-2): science requirements, concept, and implementation, Remote Sens. Environ., 190, 260-273, https://doi.org/10.1016/j.rse.2016.12.029, 2017.

Morison, J.H., Hancock, D., Dickinson, S., Robbins, J., Roberts, L., Kwok, R., Palm, S.P., Smith, B., Jasinski, M.F., and the ICESat-2 Science Team: ATLAS/ICESat-2 L3A ocean surface height, version 5. Boulder, Colorado USA. NASA National Snow and Ice Data Center Distributed Active Archive Center, https://doi.org/10.5067/ATLAS/ATL12.005, 2021.

Mulet, S., Rio, M.H., Etienne, H., Artana, C., Cancet, M., Dibarboure, G., Feng, H., Husson, R., Provost, C., and Strub, P.T.: The new CNES-CLS18 global mean dynamic topography, Ocean Sci., 17(3), 789-808, https://doi.org/10.5194/os-17-789-2021, 2021.

Passaro, M., Rose, S.K., Andersen, O.B., Boergens, E., Calafat, F.M., Dettmering, D., and Benveniste, J.: ALES+: Adapting a homogenous ocean retracker for satellite altimetry to sea ice leads, coastal and inland waters, Remote Sens. Environ., 211, 456-471, https://doi.org/10.1016/j.rse.2018.02.074, 2018.

Rapp, R.H., Yi, Y., and Wang, Y.M.: Mean sea surface and geoid gradient comparisons with Topex altimeter data, J. Geophys. Res., 99(C12), 24657–24668, https://doi.org/10.1029/94JC00918, 1994.

Sandwell, D.T., Harper, H., Tozer, B., and Smith, W.H.F.: Gravity field recovery from geodetic altimeter missions, Adv. Space Res., 68, 1059–1072, https://doi.org/10.1016/j.asr.2019.09.011, 2021.

Sandwell, D.T., and Smith, W.H.F.: Marine gravity anomaly from Geosat and ERS-1 satellite altimetry, J. Geophys. Res.: Solid Earth, 102(B5), 10039-10054, https://doi.org/10.1029/96JB03223, 1997.

Sandwell, D.T., Müller, R.D., Smith, W.H., Garcia, E., and Francis, R.: New global marine gravity model from CryoSat-2 and Jason-1 reveals buried tectonic structure, Science, 346(6205), 65-67. https://doi.org/10.1126/science.1258213, 2014.

Stammer, D., Ray, R.D., Andersen, O.B., Bosch, W., Carrère, L., Cheng, Y., Chinn, D.S., Dushaw, B.D., Egbert, G.D., Erofeeva, S.Y., Fok, H.S., Green, J.A.M., Griffiths, S., King, M.A., Lapin, V., Lemoine, F.G., Luthcke, S.B., Lyard, F., Morison, J., Müller, M., Padman, L., Richman, J.G., Shriver, J.F., Shum, C.K., Taguchi, E., Yi, Y.: Accuracy assessment of global barotropic ocean tide models, Rev. Geophys., 52(3), 243–282, https://doi.org/10.1002/2014rg000450, 2014.

Tscherning, C.C., and Rapp, R.H.: Closed covariance expressions for gravity anomalies, geoid undulations, and deflections of the vertical implied by anomaly degree variance models (208), Retrieved from Ohio State University, Columbus, 1974.

Vignudelli, S., Birol, F., Benveniste, J., Fu, L.L., Picot, N., Raynal, M., and Roinard, H.: Satellite altimetry measurements of sea level in the coastal zone. Surveys in Geophysics, 40(6), 1319-1349, https://doi.org/10.1007/s10712-019-09569-1, 2019.

Vignudelli, S., Kostianoy, A.G., Cipollini, P., and Benveniste, J.: Coastal altimetry. Springer: Heidelberg Dordrecht, Germany; London, UK; New York, NY, USA, 2011.

Wan, X., Hao, R., Jia, Y., Wu, X., Wang, Y., and Feng, L.: Global marine gravity anomalies from multi-satellite altimeter data, Earth, Planets and Space, 74(1), 1-14, https://doi.org/10.1186/s40623-022-01720-4, 2022.

Wang, B., and Sneeuw, N.: Crossover adjustment of ICESat-2 satellite altimetry for the Arctic region, Adv. Space Res., ISSN 0273-1177, https://doi.org/10.1016/j.asr.2023.07.041, 2023.

Wang, C., Wang, B., Deng, Z., Fu, M.: A Delaunay triangulation-based matching area selection algorithm for underwater gravity-aided inertial navigation, IEEE/ASME Trans. Mechatronics, 26(2), 908-917, https://doi.org/10.1109/TMECH.2020.3012499, 2020.

Wang, T., Fang, Y., Zhang, S., Cao, B., and Wang, Z.: Biases Analysis and Calibration of ICESat-2/ATLAS Data Based on Crossover Adjustment Method, Remote Sens., 14(20), 5125, https://doi.org/10.3390/rs14205125, 2022.

Watts, A.B., Tozer, B., Harper, H., Boston, B., Shillington, D.J., and Dunn, R.: Evaluation of shipboard and satellite-derived bathymetry and gravity data over seamounts in the Northwest Pacific Ocean, J. Geophys. Res.: Solid Earth, 125, 1-18, https://doi.org/10.1029/2020JB020396, 2020.

Wu, Y., Abulaitijiang, A., Featherstone, W.E., McCubbine, J.C., and Andersen, O.B.: Coastal gravity field refinement by combining airborne and ground-based data, J. Geodesy, 93(12), 2569-2584, https://doi.org/10.1007/s00190-019-01320-3, 2019.

Yu, D., Hwang, C., Andersen, O.B., Chang, E.T., and Gaultier, L.: Gravity recovery from SWOT altimetry using geoid height and geoid gradient, Remote Sens. Environ., 265, 112650, https://doi.org/10.1016/j.rse.2021.112650, 2021.

Yu, Y., Sandwell, D.T., Gille, S.T., and Villas Bôas, A.B.: Assessment of ICESat-2 for the recovery of ocean topography, Geod. J. Int., 226(1), 456-467, https://doi.org/10.1093/gji/ggab084, 2021.

Yuan, J., Guo, J., Zhu, C., Li, Z., Liu, X., Gao, J.: SDUST2020 MSS: A global 1'× 1' mean sea surface model determined from multi-satellite altimetry data, Earth Syst. Sci. Data, 15(1), 155-169, https://doi.org/10.5194/essd-15-155-2023, 2023.

Zaki, A., Magdy, M., Rabah, M., and Saber, A.: Establishing a marine gravity database around Egypt from satellite altimetry-derived and shipborne gravity data, Mar. Geod., 45(2), 101-120, https://doi.org/10.1080/01490419.2021.2020185, 2022.

Zhang, S., Abulaitijiang, A., Andersen, O.B., Sandwell, D.T., and Beale, J.R.: Comparison and evaluation of high-resolution marine gravity recovery via sea surface heights or sea surface slopes, J. Geodesy, 95, 66, https://doi.org/10.1007/s00190-021-01506-8, 2021.

Zhang, S., Zhou, R., Jia, Y. Jin, T., and Kong, X.: Performance of HaiYang-2 altimetric data in marine gravity research and a new global marine gravity model NSOAS22, Remote Sens., 14(17), 4322, https://doi.org/10.3390/rs14174322, 2022.

Zhu, C., Guo, J., Gao, J., Liu, X., Hwang, C., Yu, S., Yuan, J., Ji, B., and Guan, B.: Marine gravity determined from multi-satellite GM/ERM altimeter data over the South China Sea: SCSGA V1.0, J. Geodesy, 94, 50, https://doi.org/10.1007/s00190-020-01378-4, 2020.

Zhu, C., Guo, J., Yuan, J., Li, Z., Liu, X., and Gao, J.: SDUST2021GRA: Global marine gravity anomaly model recovered from Ka-band and Ku-band satellite altimeter data, Earth Syst. Sci. Data, 14(10), 4589-4606, https://doi.org/10.5194/essd-14-4589-2022, 2022.

Zingerle, P., Pail, R., Gruber, T., and Oikonomidou, X.: The combined global gravity field model XGM2019e, J. Geodesy, 94, 66, https://doi.org/10.1007/s00190-020-01398-0, 2020.